Available online at www.sciencedirect.com
SCIENCE DIRECT
Journal of volcanology and geothermal research
Journal of Volcanology and Geothermal Research 151 (2006) 319–339
www.elsevier.com/locate/jvolgeores

The effects of conduit length and acoustic velocity on conduit resonance: Implications for low-frequency events

Susan Sturton, Jürgen Neuberg *

School of Earth Sciences, The University of Leeds, Leeds LS2 9JT, UK

Received 5 October 2004; received in revised form 9 September 2005; accepted 15 September 2005
Available online 23 November 2005

Abstract

Low-frequency seismic events at volcanoes are modelled as the seismic wavefield from a magma-filled conduit embedded in a solid country rock using a finite difference method. The effects of varying the conduit length and the impedance contrast between the magma and the country rock are examined, generating a range of possible signals. Short-windowed spectrograms are used to look at the time–frequency relationships within the events in detail, and some of the possible variations are identified using a series of schematic spectrograms. The numerical results are compared to examples of observed seismic data from Soufrière Hills Volcano, Montserrat. While the spectra of the observed events are often different to the spectra of the numerical results, the spectrograms have similar features and show that the low-frequency events from Montserrat are composed of discrete subevents.

Keywords: low-frequency volcanic events; Montserrat; spectrograms; conduit length; acoustic velocity; numerical modelling

1. Introduction

Low-frequency events are seen at many volcanoes including Arenal (Hagerty et al., 2000), Montserrat, West Indies (Miller et al., 1998), Karymsky, Russia (Johnson and Lees, 2000) and Erebus, Antarctica (Rowe et al., 2000). Low-frequency seismic events are important for forecasting volcanic hazard due to their occurrence in swarms prior to eruptions (Chouet, 1996; Miller et al., 1998). Their duration can last from a few seconds up to a minute. Additionally, low-frequency events differ in their onset (presence or absence of a high-frequency component) and in their shape.

Numerical models are used to try to explain the differences between the seismic events. Modelling of low-frequency events has focused on the idea that the seismicity is the result of a seismic resonance in a fluid-filled body because of the low-frequency content and sharply defined spectral peaks of the events.

The most simple physical explanation for low-frequency events is that of free eigenvibrations of a fluid or gas volume, for which there is no coupling between the fluid and the solid (Schlindwein et al., 1995; Benoit and McNutt, 1997). Models of the eigenvibrations of a freely oscillating fluid do not incorporate the coupling between the acoustic vibration in the fluid with the surrounding solid. In contrast, analytical solutions for interface waves trapped in a fluid-filled infinite layer are derived by Ferrazzini and Aki (1987). Two types of interface waves exist:

1. Slow waves travelling at velocities lower than the acoustic velocity, approaching the Stonely wave at a liquid–solid interface for short wavelengths.

* Corresponding author.
E-mail address: locko@earth.leeds.ac.uk (J. Neuberg).

0377-0273/$ - see front matter © 2005 Elsevier B.V. All rights reserved.
doi:10.1016/j.jvolgeores.2005.09.009

2. Fast waves travelling with phase velocities between the acoustic velocity and the *S*-wave velocity outside the crack.

Both slow and fast waves are dispersive. The phase velocity of slow waves decreases with increasing wavelength which in this study is referred to as inverse dispersion while the phase velocity of fast waves increases with wavelength.

Slow waves have been identified in numerical models for both a crack and a conduit. Chouet (1986) and Chouet (1988) consider the resonance of a fluid-filled crack, modelling both the acoustic resonance in the fluid and the coupling with the surrounding solid using a finite difference method. The seismic waves travel as slow waves (called crack waves by the author) along the interface of the crack. The interface waves radiate into the country rock at the antinodes. The phase velocity decreases as the wavelength increases so the spectrum is not composed of equally spaced peaks but the peaks become more closely spaced as the frequency increases. However, due to the exponential decay of the interface waves (Ferrazzini and Aki, 1987), it is unlikely that the resonances described in these papers could be observed away from the crack. Because of the decay it would not be possible to construct a seismogram at surface resulting from the interface waves.

Sturton (2003) and Jousset et al. (2003), using the same method as Neuberg et al. (2000), show that the ends of a wide conduit act as secondary sources as suggested by Ferrazzini and Aki (1987). The slow wave is found to travel along the conduit and when it reaches the ends it is partially reflected back along the conduit and partially transmitted into the country rock. Each low-frequency event can therefore be considered to be composed of a series of subevents. The radiating of the waves into the country rock is not subject to the same sort of decay as the interface waves and can therefore be recorded at the surface using seismometers. Jousset et al. (2003) concentrates on producing spectra similar to the observed data.

This study follows the method of Neuberg et al. (2000). The same finite difference method is used to model the effects of conduit length and impedance contrast, to understand the influence of these parameters on the seismic signal. Frequencies obtained from the numerical model are compared to organ-pipe modes, and frequencies for interface wave, showing that the wave is dispersive and travels slower than the acoustic velocity. Dispersion is identified in the subevents using short-windowed spectrograms which examine the time–frequency behaviour of the numerical results in more detail. The dispersion characteristics of the signals provide a method of distinguishing a model with fast velocities and a long conduit from a model with slow velocities and a short conduit. The numerical results are combined to develop 'schematic spectrograms' which illustrate the main features of spectrograms for different parameters. These are compared with spectrograms of observed data from Montserrat to explain the differences between a few examples of low-frequency events on the basis of the numerical results. There are some differences between the models and the observed data because nature is more complicated, and explanations for the differences are provided.

The model is two-dimensional and therefore the only geometry that can be modelled is a fluid-filled dyke. In this paper, this is nonetheless referred to as a conduit to emphasise that the choice of parameters is specifically applicable to volcanic systems.

2. Description of finite difference method

A finite difference method is used to solve the elastic equations of motion in two dimensions using a staggered grid method given by Levander (1988). The formulation uses a fourth-order central spatial discretisation and a leap-frog method time discretisation and is fourth-order accurate in space and second-order accurate in time (Levander, 1988). Free surface boundary conditions are imposed at the top of the domain by setting the stresses at all the grid points above and on the free surface to zero (Levander, 1988). The free-surface boundary conditions are applied at four grid points from the top of the domain. To limit reflections of the seismic waves from the sides and bottom of the grid, an attenuative zone of exponential damping is applied to a region 50 grid points wide along these three edges of the grid (Cerjan et al., 1985).

Fig. 1 shows the setup of the finite difference code. A liquid-filled rectangle is surrounded by the solid. The conduit is assumed to contain a fluid with different seismic parameters to the surrounding elastic medium. Within the conduit, the elastic parameters of the magma are used, and outside the conduit, elastic parameters of the country rock. There are no explicit conduit boundary conditions and the stress tractions are continuous throughout the medium. A source wavelet term is added to the pressure term inside the liquid, placed 100 m below the top of the conduit in the middle between the side walls, to trigger the seismic wavefield. At the stress-free surface seismometers, marked as triangles,

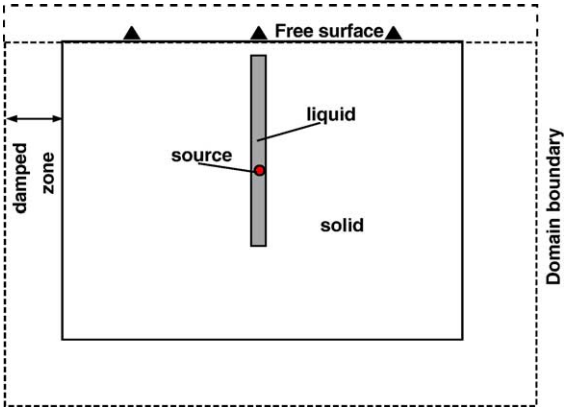

Fig. 1. Set up of the finite difference model. The conduit is a rectangle surrounded by country rock. The source signal, drawn as a circle, triggers the resonance from inside the conduit. The seismometers (triangles), record the signal at the free surface.

'record' the vertical and horizontal component of the velocity. The code is run with equal horizontal and vertical grid spacing of 1 m and a timestep of 0.0001 s. The grid is 1400 m wide and 2000 m deep.

The liquid-filled cuboid represents a magma-filled conduit inside a solid volcanic edifice. At volcanoes such as Montserrat, the viscosity of the magma increases at the top of the conduit due to the exsolution of gas and a solid plug develops. This defines the top end of the 'fluid-filled conduit'. The seismometer is placed 500 m away from the top of the conduit.

The bottom end of the conduit is cut off sharply and is therefore a strong reflector as shown by Jousset et al. (2003). At a volcano, a conduit might extend from the surface to a magma chamber a few kilometres deep. However, a strong reflector could also be the result of a sudden bend in the conduit or inhomogeneities in both the country rock or magma. Therefore, rather than always considering the entire length of the resonating conduit as the distance from the surface to the magma chamber, the conduit length is defined as a variable because it will depend on the distance between any inhomogeneities that are strong reflectors of the seismic wave.

The source signal used throughout this study, unless otherwise stated, is a delta-pulse filtered with a 1–5 Hz band-passed filter (Fig. 2). This signal contains very similar frequencies to low-frequency events and is therefore used to produce events with frequencies directly comparable with observed data. The numerical results then show the influence of conduit parameters on such a signal.

3. Comparison of three models of wave propagation

In this section, frequencies obtained from the numerical solutions are compared to solutions for organ-

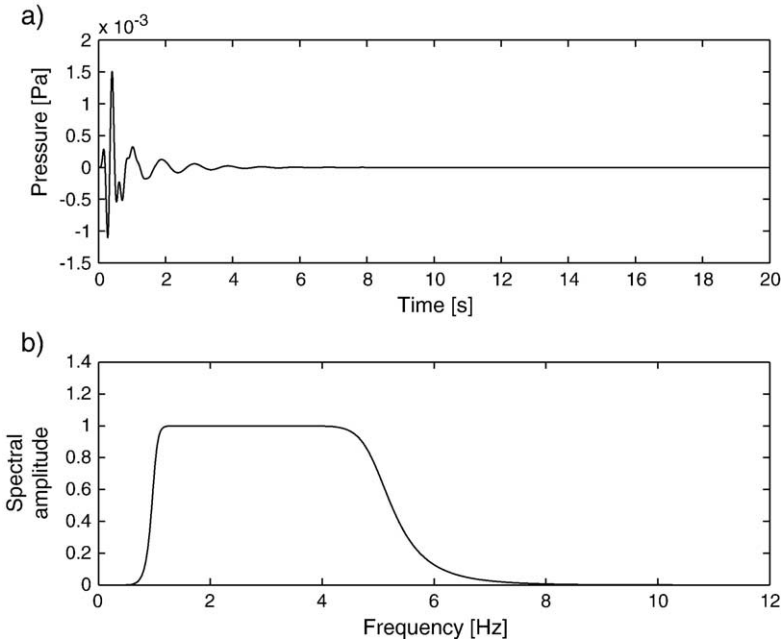

Fig. 2. Time series and Fourier transform of a delta pulse filtered with a 1–5-Hz band pass filter. The signal lasts about 6 s. It contains frequencies between 0.5 and 8 Hz although the highest amplitude frequencies are between 1 and 5 Hz. The lower cutoff is quite sharp occurring over about 1 Hz. The higher cutoff is more shallow.

pipe modes and interface waves. The frequency, f, of a closed organ-pipe mode with wavelength equal to the length of the conduit is given by

$$f = \frac{c}{L} \tag{1}$$

where c is the acoustic velocity in the fluid and L is the length of the conduit.

Ferrazzini and Aki (1987) derive the dispersion relations for slow waves trapped in a fluid layer expressed in terms of ratios of phase velocity to seismic velocity, $\varepsilon_s = v/\beta$, $\varepsilon_c = v/\alpha$ and $\varepsilon = v/c$ where the phase velocity of the trapped wave is v, c is the acoustic velocity in the fluid layer, and α and β are the P-wave velocity and the S-wave velocity in the surrounding medium. The dispersion relation for slow waves which travel at lower velocities than the acoustic velocity is

$$\tanh\left(\sqrt{1-\varepsilon^2}\,\frac{hk_x}{2}\right) = -\frac{\rho_s}{\rho_f}\,\frac{\sqrt{1-\varepsilon^2}}{\varepsilon_s^4}\left(\frac{\left(2-\varepsilon_s^2\right)^2}{\sqrt{1-\varepsilon_c^2}} - 4\sqrt{1-\varepsilon_s^2}\right) \tag{2}$$

where the width of the layer is h, ρ_s and ρ_f are the density of the solid and the fluid, respectively, and k_x is the horizontal wave number. Eq. (2) is solved for the phase velocity by employing a grid search to find values on either side of the roots of the equation, followed by a bisection method to find the root more accurately.

In the numerical simulations shown in Fig. 3, a 0.5-Hz, one-lobed Küpper wavelet is used as the source signal so that the frequency of the lowest peak in the spectrum can be measured. The lowest peak measures the frequency of the wavelength equal to the length of the conduit which can therefore be compared with both the organ-pipe modes and the analytical solutions for slow waves.

These models are now compared for a conduit 2000 m long and 30 m wide. In the surrounding elastic medium, the P-wave velocity is 3000 ms^{-1}, the S-wave velocity is 1725 ms^{-1} and the density is 2600 kg m^{-3}. The density of the magma is kept constant at 700 kg m^{-3} and the acoustic velocity is varied in the range 300–1000 ms^{-1}.

Fig. 3 shows the frequencies for each of the three models. For low acoustic velocities, the curve for the slow wave solutions converges on that of the organ-pipe modes and the slow wave travels at velocities increasingly closer to the acoustic velocity. For higher acoustic velocities, the frequencies for the slow waves are lower than that for the organ-pipe modes. The frequencies from the numerical solutions fit the analyt-

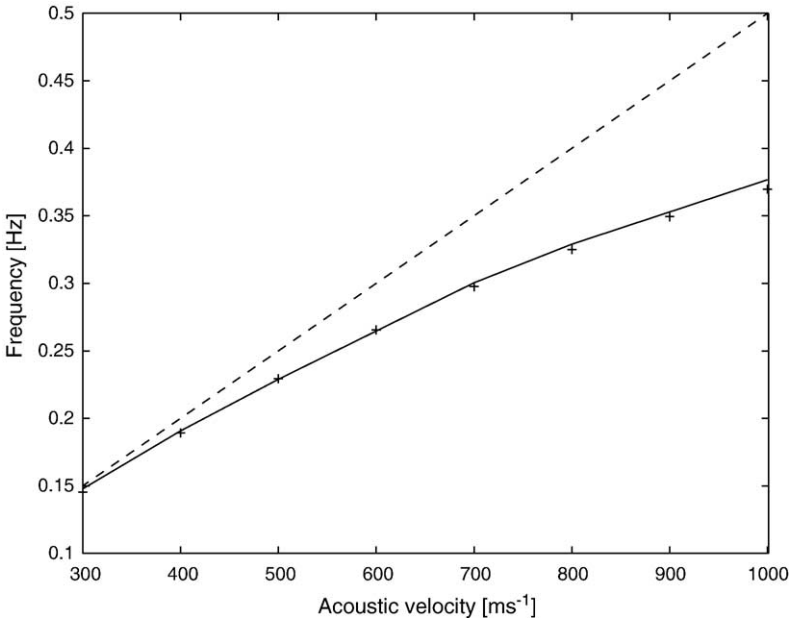

Fig. 3. Comparison of frequencies for the organ-pipe model (dashed line), analytical solution for slow waves from Ferrazzini and Aki (1987) for a wavelength equal to the conduit length (solid line) and the numerical solution (crosses). The density of the magma is 700 kg m^{-3} for all models. The numerical solutions fit the analytical solution very well, but the frequency predicted by organ-pipe modes (dashed line) deviates increasingly as the seismic velocity is increased.

ical solutions for slow waves very well showing that the numerical method is grid independent. This demonstrates that the phase velocity of the interface wave of the numerical result is well described by the analytical result unlike Chouet (1988) where the phase velocities from numerical solutions for long wavelengths in a fluid-filled crack were found to be slower than the analytical solutions.

The analytical solutions provide only a limited understanding of how the seismic waves radiate as the effects of the conduit ends are not addressed, only radiation along the sides. They do not model the amplitudes and decay of the seismic signal and there is also no way of constructing a 'seismogram', that might be recorded some distance from the interface, at the free surface. For these reasons, numerical simulations are used in the following to study the effects of conduit length and seismic parameters.

4. Parameterisation of the model

Conduit geometry: Observations of the width of major spines from Montserrat suggest a conduit width of about 30 m (Watts et al., 2002). A width of 30 m is therefore used while the conduit length is varied as discussed in Section 2. It was found that the conduit width is relatively unimportant in the range of 30–90 m that has been tested (Sturton, 2003).

Acoustic velocity and density in the conduit: The seismic parameters in the magma are assumed to be homogeneous to consider the effects of the impedance contrast. However, the seismic velocity and density do vary with the volume of 167 exsolved gas so a range of possible values are found using equations described in Neuberg and O'Gorman (2002).

The following parameters are used to find the acoustic velocity for an andesitic melt containing only water as a gaseous phase, over a range of pressures, with the water content at saturation for a given pressure: the density of the melt is 2300 kg m^{-3} (Neuberg, 2000) and the seismic velocity of the melt is 2300 ms^{-1} (Rivers and Carmichael, 1987). This gives the melt a bulk modulus of 1.21×10^{10} Pa s. The temperature of the melt is 1120 K (Devine et al., 1998). The mass fraction of water initially dissolved in the melt is 2.5 wt.%. The calculated values of pressure, volume of exsolved gas acoustic velocity and density are listed in Table 1.

Table 1
Seismic parameters used within the conduit

Pressure (MPa)	Vol. frac. exsolved	Density (kg m^{-3})	Acoustic velocity (ms^{-1})
19.6	0.299	1623	200
30.4	0.088	2100	400
34.7	0.029	2235	700
36.0	0.013	2270	1000
>37	0	2300	2400

5. Effects of conduit length

In this section, the effect of the conduit length is considered for one magma with a low impedance contrast and one magma with a high impedance contrast with the surrounding country rock. Seismograms, spectra and short-windowed spectrograms are used to compare the signals. All spectrograms are calculated using a 2-s window. The seismic properties of the country rock are kept constant. The P-wave velocity and the S-wave velocity are 3000 ms^{-1} and 1725 ms^{-1}, respectively, and the density is 2600 kg m^{-3}. The conduit is buried 100m below the free surface and the source is triggered 100 m below the top of the conduit.

Low impedance contrast: In this section, the results for a low gas volume fraction of 0.013 and therefore low impedance contrast are considered. The low exsolved gas content is representative of a deep conduit section. The magma has an acoustic velocity of 1000 ms^{-1} and a density of 2270 kg m^{-3}. The conduit length is varied between 200 m and 1500 m.

The seismogram for a short conduit, 200 m long (Fig. 4a), shows high frequencies at the start of the signal, lasting for about 0.5 s. This is followed by a monochromatic coda which dies away after about 7 s, decaying smoothly with time. The spectrum (Fig. 4b) shows two peaks, one at 2 Hz and the other much lower peak at 4.2 Hz. In the spectrogram (Fig. 5a), initially high frequencies are seen in the signal and at all times there is a high amplitude at approximately 2 Hz. This signal is composed of a wavelength similar to the length of conduit travelling at the slow wave velocity and only one frequency is present in the coda.

When the conduit is 500 m long, the signal no longer has a monochromatic coda (Fig. 4c). The spectrum (Fig. 4d) shows five equally spaced peaks, less than 1 Hz apart. In a spectrogram with a 1.2-s window (Fig. 5b), individual subevents originating from the top of the conduit, and building up the signal can be distinguished. In the seismogram, there are no obvious repeated subevents. These are spaced at 1-s intervals and show inverse dispersion with the high frequencies arriving before the low frequencies. The subevents overlap in time which is why they cannot be resolved in the seismogram.

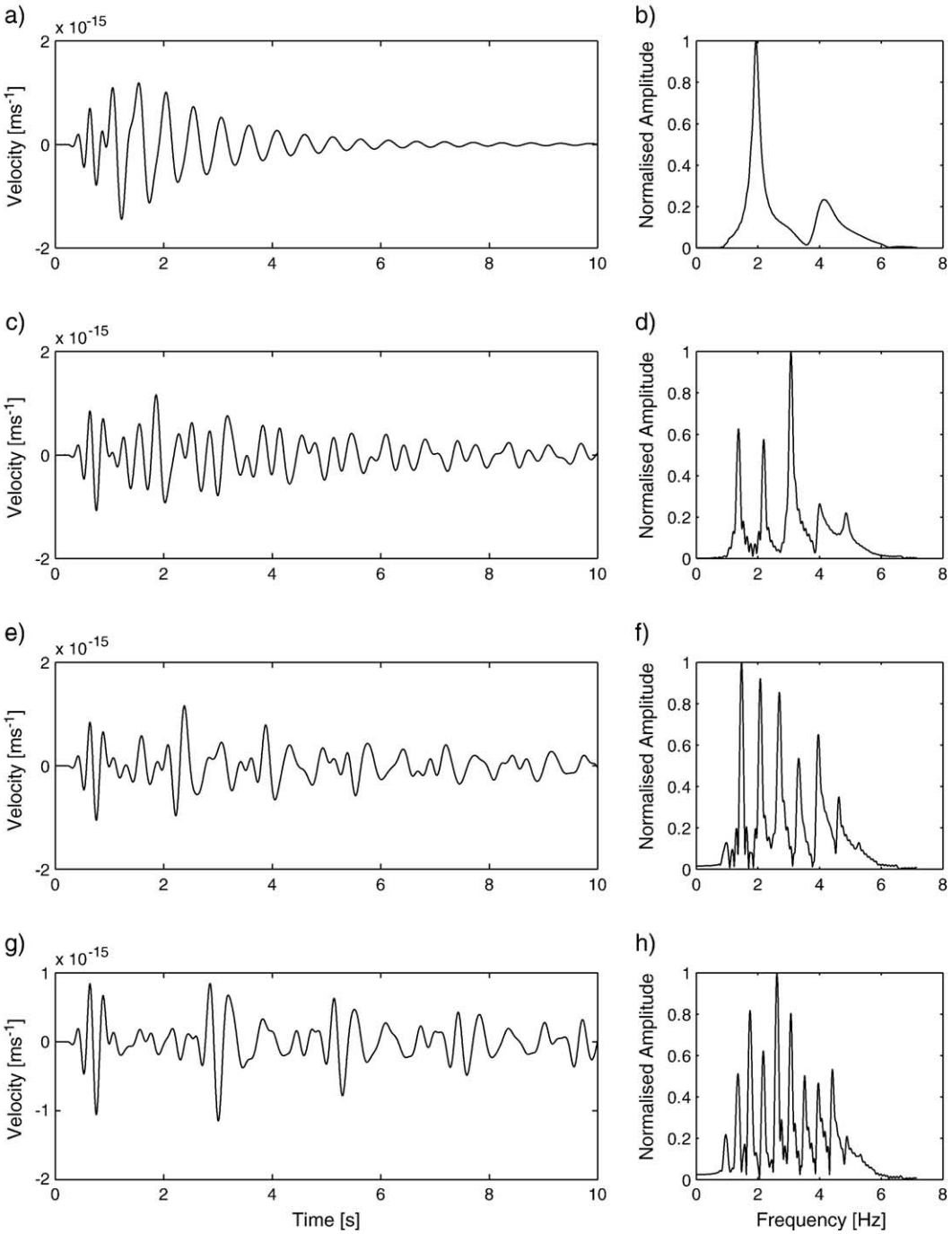

Fig. 4. Seismograms and spectra for properties consistent with a gas volume fraction of 0.013 and a conduit length of (a and b) 200 m, (c and d) 500 m, (e and f) 1000 m and (g and h) 1500 m. For a short conduit only one frequency is present in the coda of the event: this frequency has a wavelength equal to the length of the conduit. As the conduit is made longer, the events from the top of the conduit arrive at greater time intervals so are more easily resolved.

After a further increase in length to 1000 m, the subevents making up the signal can be resolved in the seismogram (Fig. 4e) arriving at slightly less than 2-s intervals. The dispersion is seen in both the seismogram and the spectrogram (Fig. 5c), the high frequencies travelling faster than the low frequencies. The subevents are more widely separated than for the 500-m-long conduit.

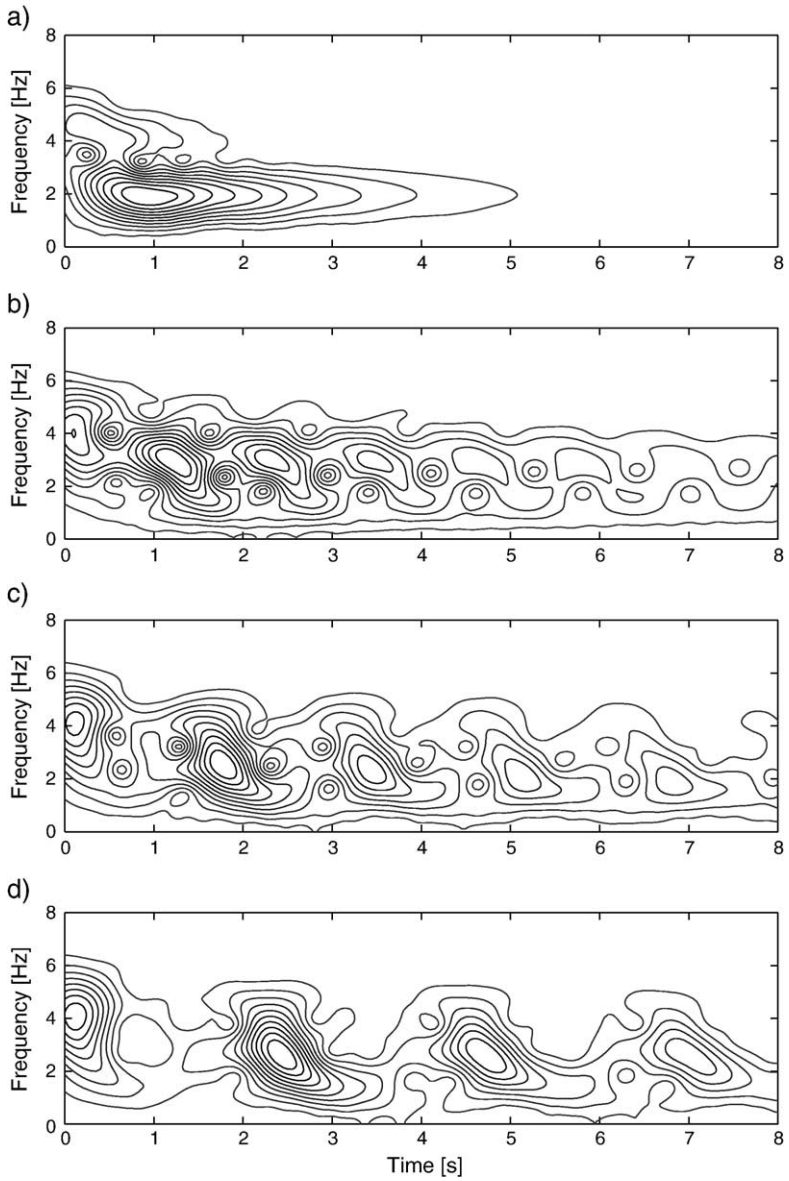

Fig. 5. Spectrograms for properties consistent with a gas volume fraction of 0.013 and a conduit length of (a) 200 m, (b) 500 m, (c) 1000 m and (d) 1500 m. For a short conduit only one frequency is present in coda of the event. As the conduit is made longer, the events from the top of the conduit arrive at greater time intervals so are more easily resolved. These events show inverse dispersion with the low frequencies arriving later than the high frequencies.

For a conduit length of 1500 m, subevents are more easily resolved in the seismogram (Fig. 4g). Subevents arrive over 3 s apart and dispersion is observable in both the seismogram and spectrogram (Fig. 5d). The spacing of the spectral peaks in the spectrum of the whole event shows a further decrease to 0.3 Hz (Fig. 4h).

High impedance contrast: The results for an exsolved gas volume fraction of 0.088 and therefore a higher impedance contrast are now considered. This gas volume fraction is representative of shallower depths. The magma in this case has an acoustic velocity of 400 ms^{-1} and a density of 2270 kg m^{-3}.

For a 200-m-long conduit, the seismic signal can be split into subevents (Fig. 6a) but the first onset of each event is not clear. Unlike the previous example in Fig. 4a, the signal is not monochromatic, and rather than decaying smoothly with time, is composed of cyclic waveforms that gradually decrease in amplitude, resulting in a pulsating signal. The start of the event does not contain

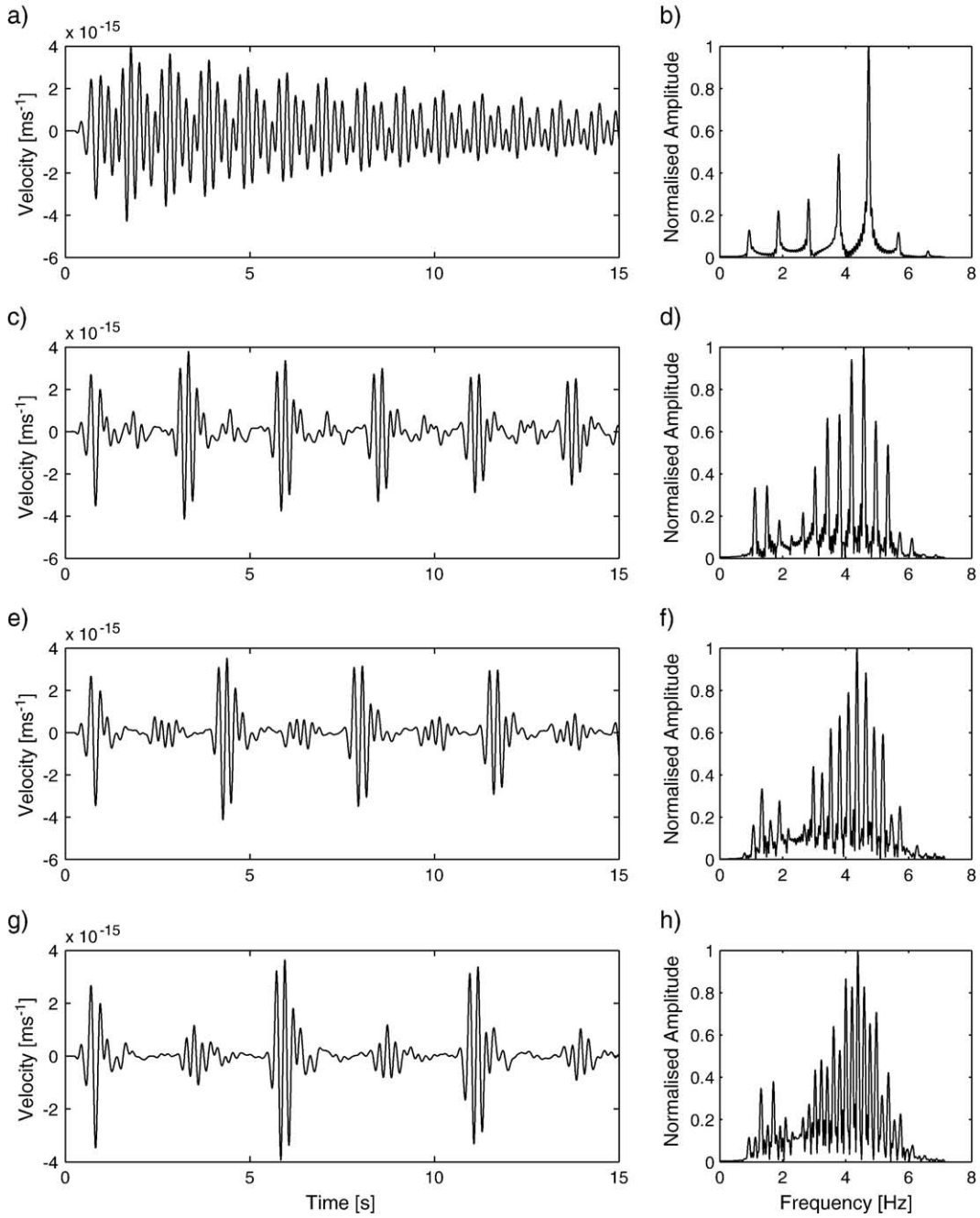

Fig. 6. Seismograms and spectra for properties consistent with a gas volume fraction of 0.088 and a conduit length of (a and b) 200 m, (c and d) 500 m, (e and f) 1000 m and (g and h) 1500 m. When the conduit is short the subevents are closely merged. As the conduit is made longer the subevents become separable and smaller subevents from the bottom of the conduit can be seen.

higher frequencies than the rest of the event. The spectrum shows a series of spectral peaks, with a spacing of 1.1 Hz. In the spectrogram (Fig. 7a), the pulses show as peaks at 4.5 Hz spaced approximately every second.

Once the conduit length is increased to 500 m, individual subevents can be separated in the seismogram (Fig. 6c), arriving every 2.5 s. In the spectrum, the spacing of the spectral peaks is 0.4 Hz (Fig. 6d). In the spectrogram (Fig. 7b), the subevents are seen every 2.5 s. Within each subevent, all frequencies arrive at the same time so there is no dispersion.

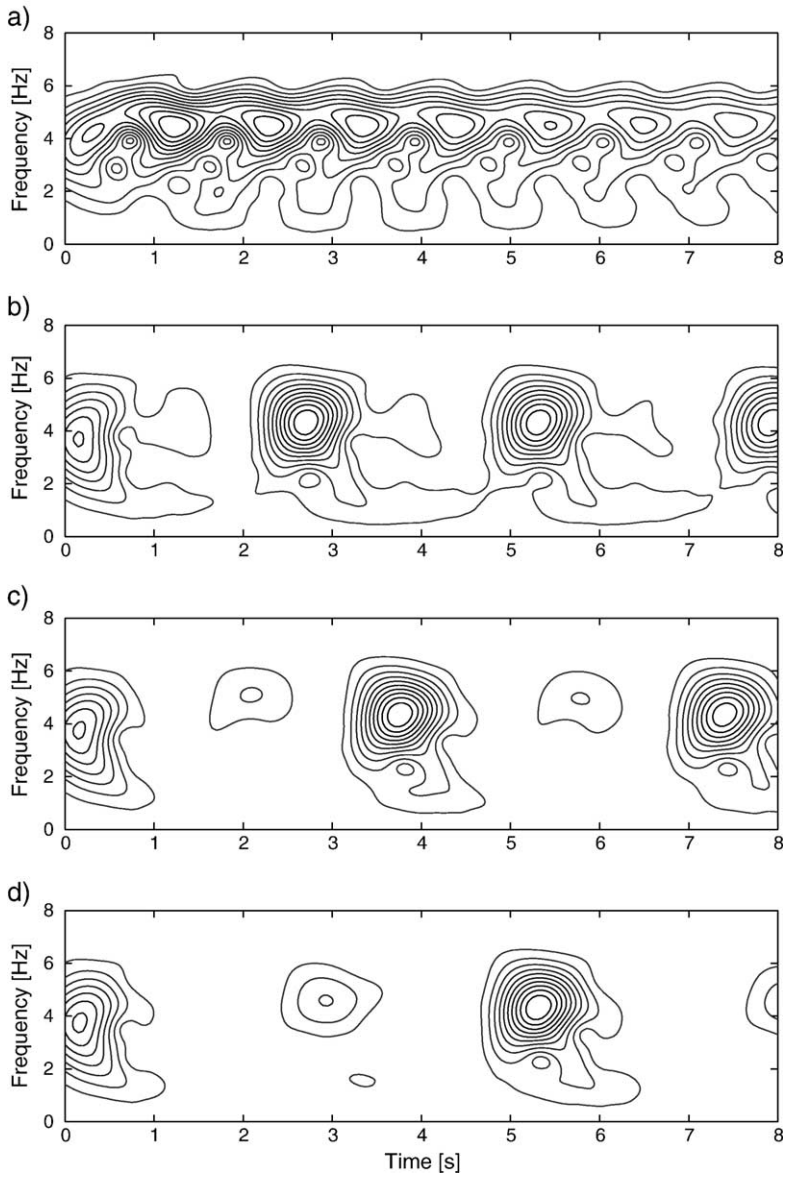

Fig. 7. Spectrograms for properties consistent with a gas volume fraction of 0.088 and a conduit length of (a) 200 m, (b) 500 m, (c) 1000 m and (d) 1500 m. For a short conduit, the spectrogram shows a continuous oscillation which can be separated into subevents. The subevents for this acoustic velocity do not show dispersion.

For a conduit length of 1000 m, two types of subevent can be observed in the seismograms (Fig. 6e). Every 4 s, there is a subevent similar to those in the previous seismogram. In between there are subevents with an amplitude about a tenth of the higher amplitude events which can also be seen in the 500-m-long conduit. Neither type of subevent shows dispersion (Fig. 7c). The spectrum has spectral peaks every 0.2 Hz.

A final increase of the length of the conduit to 1500 m and both sets of subevents are present but arrive at time intervals of 5 s (Fig. 6g). The spectral peaks are every 0.19 Hz (Fig. 6h).

6. Effects of seismic parameters on dispersion

The models where the conduit length and seismic parameters result in a frequency spacing of approximately 0.5 Hz are compared. A frequency of 0.5 Hz is chosen for the comparison because at this frequency events are spaced at 2-s intervals which is easy to

resolve. The conduit lengths and seismic properties are summarised in Table 2.

Fig. 8 shows the seismograms for each combination and Fig. 9 shows the spectrograms of the seismograms. For the shortest conduit of 200 m, in the seismogram (Fig. 8a), the decay of the subevents is very gradual and barely noticeable over the length of the signal. The spectrogram (Fig. 9a) shows repeated, almost identical subevents.

When the conduit length is 400 m and the acoustic velocity is 400 ms^{-1}, the subevents making up the signal no longer merge (Fig. 8b). Each subevent arrives about 2 s after the previous subevent. Again the spectrogram (Fig. 9b) is composed of repeated, almost identical subevents. Most frequencies travel at approximately the same velocity. These first two signals show little dispersion.

As the length of the conduit and the seismic velocities are further increased, the dispersion becomes apparent with the high frequencies arriving earlier than the low frequencies. This is seen in the spectrograms of Fig. 9c, d and e. As the impedance contrast decreases, the dispersion increases. This is observed by examining the time delay between the arrival of the high frequencies and low frequencies of the events. The effect is larger for later subevents. In Fig. 9c, the high frequencies of the fourth subevent arrive after 6.2 s and the low frequencies after 7.2 s, a time delay of 1 s. In Fig. 9d, there is a time delay of 1.5 s and in Fig. 9e of about 2 s.

As the impedance contrast increases, the signal decays more rapidly. In Fig. 8b, there is a slight decay with time. For Fig. 8e, the signal has decayed to less than half the initial amplitude after 10 s.

6.1. Summary and explanation of the numerical results

In this section, the main trends shown by the numerical simulations are explained. The seismograms are also further characterised to show how the subevent spacing and the velocity of the interface waves vary over the range of seismic parameters in Table 1 and for conduit lengths between 200 and 1500 m.

Table 2
The combination of conduit length and seismic properties required to produce spectral peaks spaced 0.5 Hz apart

Length (m)	Vol. frac. exsolved	Seismic velocity (ms^{-1})
200	0.299	200
400	0.088	400
700	0.029	700
850	0.013	1000
1250	0	2400

The following method is used to characterise the seismic events: The average spacing of the peaks in the spectrum is calculated by taking the difference between the lowest peak and the highest peak and dividing by the number of peaks. This method averages over the slight differences in the peak spacing in different parts of the spectrum. The reciprocal of the average spacing of the spectral peaks gives the average spacing of the subevents in the timeseries. This method of measuring the spacing of the subevents is especially useful if the subevents are very closely merged and the first onset is unclear. The average velocity with which the wave travels in the conduit is given by

$$v_{av} = \frac{2L}{t_{av}} \tag{3}$$

where v_{av} is the average velocity, L is the length of the conduit and t_{av} is the average spacing of the subevents in the timeseries. Fig. 10 shows the results for the spacing of the spectral peaks, the average subevent spacing and the average velocity plotted against the length of the conduit for the seismic properties sets given in Table 1.

Spacing of subevents: If the conduit is made longer or the acoustic velocity is reduced the subevents arrive at longer time intervals (Fig. 10b) because the seismic wave takes more time to travel the length of the conduit. The increase in the spacing of the events is approximately linear with conduit length (Fig. 10b). When the conduit is made very short the subevents become so closely merged that they cannot be easily separated (Fig. 7a) and finally the event is composed of a monochromatic oscillation (Fig. 5a).

Spectra: All the spectra show a series of equally spaced, sharply defined peaks (Figs. 4 and 6). The spacing of the spectral peaks decreases if the conduit length increases or if the acoustic velocity is reduced (Fig. 10a). The seismic signals are composed of a series of regularly spaced, similar subevents and therefore can be considered to be a series of spikes spaced at time intervals, δt, convolved with a source signal. The spectrum of such a signal consists of regularly spaced peaks with the spacing, δf, related to δt by

$$\delta f = \frac{1}{\delta f} \tag{4}$$

(Schlindwein et al., 1995; Powell and Neuberg, 2003). The envelope of the spectrum is determined by the source spectrum. The spacing of the spectral peaks is therefore controlled by the spacing of the subevents. If the conduit is made longer or the

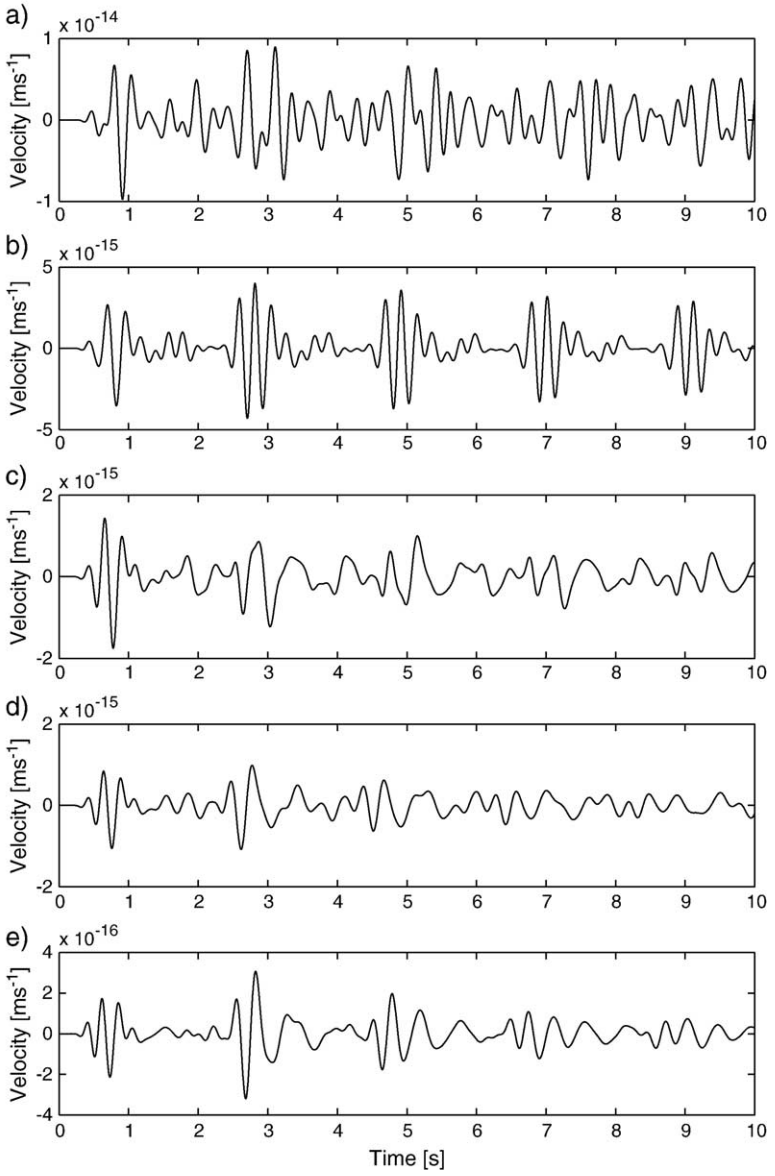

Fig. 8. Seismograms for (a) a conduit length of 200 m and seismic velocity of 200 ms^{-1}, (b) 400 m and 400 ms^{-1}, (c) 700 m and 700 ms^{-1}, (d) 850 m and 1000 ms^{-1} and (e) 1250 m and 2400 ms^{-1}. As the conduit becomes longer and the seismic velocity higher, the signal decays more rapidly and some dispersion in the separate events becomes evident.

acoustic velocity decreases the subevents are more widely spaced and so the spacing of the spectral peaks decreases.

The spectra in Fig. 6d, f and h show a further feature. The band widths of the spectra are between 1 and 7 Hz, similar to the bandwidth of the source signal (Fig. 2b). However, the spectral peaks do not all have the same amplitude with the high amplitude at around 4 Hz and low amplitudes at just above 2 Hz. This is because the spectra are further modified by the position of the source in the conduit. If the source is at the top of the conduit, there will only be a downward travelling wave and subevents caused by this wave will be equally spaced in time. If the source is placed just a short distance from the top there will be an upward and a downward travelling wave. These will produce closely spaced pairs of subevents. Fig. 11 shows the effect of this on the spectra. When the subevents are equally spaced (Fig. 11a), the spectral peaks are equally spaced and have the same amplitude (Fig. 11b). In Fig. 11c, the spikes arrive every 1 s in pairs 0.2 s apart. The spectrum (Fig. 11d) shows spectral peaks every 1 Hz but the

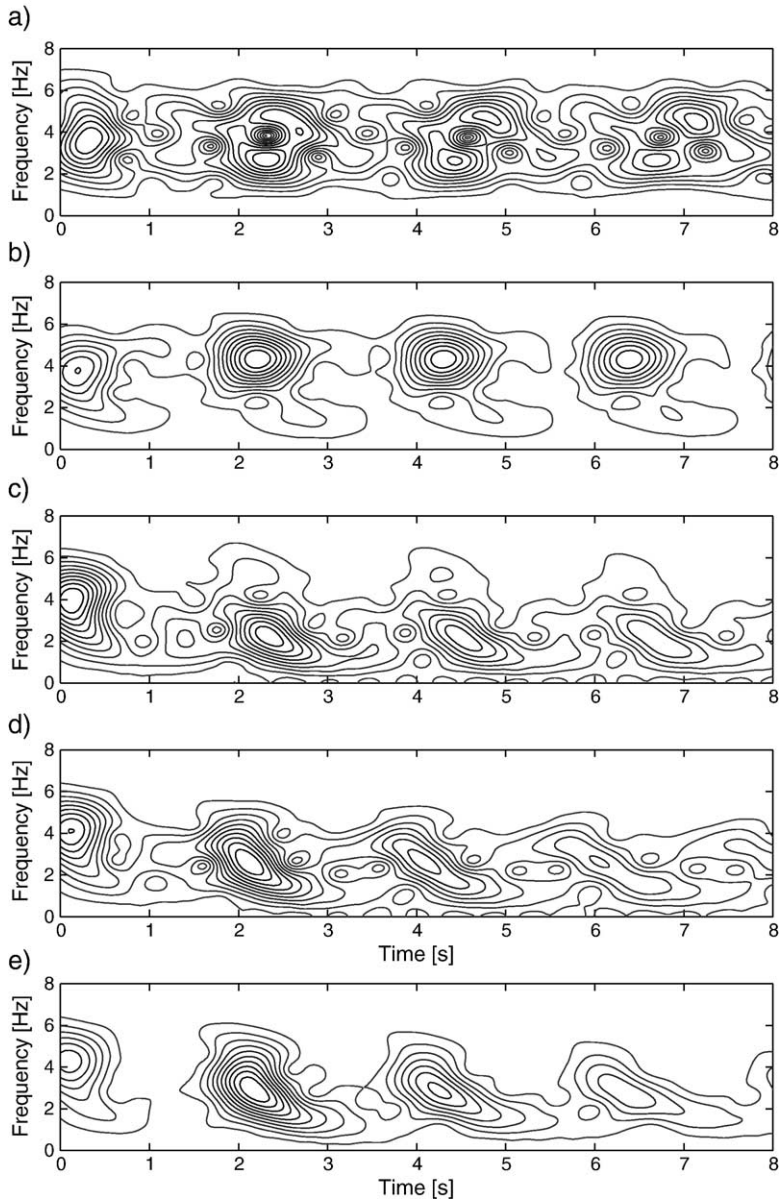

Fig. 9. Spectrograms for the seismograms in Fig. 8 for (a) a conduit length of 200 m and seismic velocity of 200 ms^{-1}, (b) 400 m and 400 ms^{-1}, (c) 700 m and 700 ms^{-1}, (d) 850 m and 1000 ms^{-1} and (e) 1250 m and 2400 ms^{-1}. All the spectrograms consist of a series of equally spaced events arriving at approximately the same time. As the seismic velocity inside the conduit increases, there is more dispersion in the signal.

amplitude of the peaks are modified with a pattern of spectral peaks every 5 Hz superimposed.

The pattern in the amplitude of the spectral peaks in the spectra in Fig. 6 is the result of pairs of subevents arriving at very short time intervals. The source is 100 m from the top of the conduit producing pairs of subevents with a spacing of 0.25 s if the acoustic velocity is 400 ms^{-1}. The spectral peaks (e.g. Fig. 6f) show a maximum amplitude at approximately 4 Hz.

Dispersion within the subevents: As the acoustic velocity inside the conduit increases, lower frequencies travel slower than high frequencies and inverse dispersion is observed in the spectrograms. In Fig. 10c, the average velocities for the different seismic parameters are compared with each other. Although the average velocity is higher if the acoustic velocity in the conduit is higher, it is lower relative to the acoustic velocity. For an acoustic velocity of 200 ms^{-1}, the average velocity equals the acoustic velocity. When the acoustic velocity

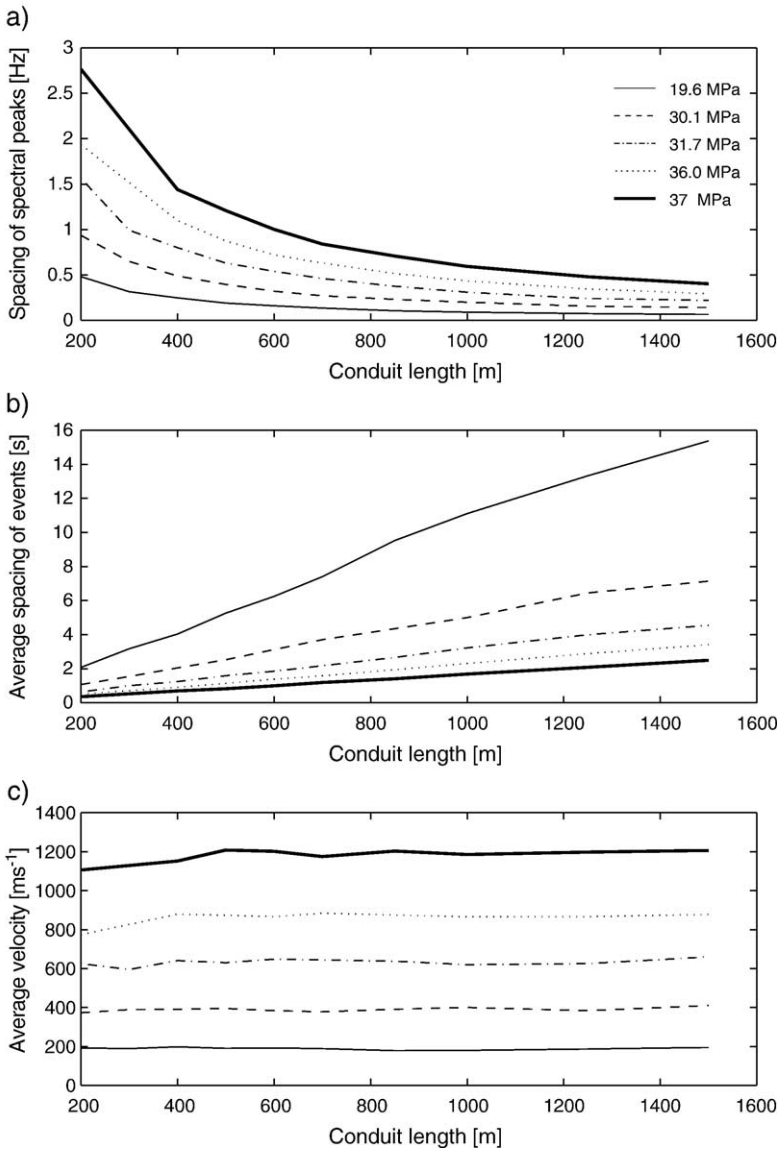

Fig. 10. The effect of seismic parameters on (a) the spacing of peaks in frequency, (b) the average spacing of events and (c) the average velocity with which the wave travels in the conduit. A longer conduit increases the spacing of the events because the seismic wave has to travel further along the conduit before it reaches the top again. As the acoustic velocity decreases, the event spacing increases because the wave travels slower in the conduit. The average velocity is lower relative to the acoustic velocity when the acoustic velocity is high and the signal is more dispersive.

is 2400 ms^{-1}, the average velocity is half the value of the acoustic velocity. Therefore, when the subevents show dispersion the slow wave travels at a relatively lower velocity compared to the acoustic wave. For the higher acoustic velocities, there is also more dispersion in the subevents (Fig. 9). Therefore, dispersion allows us to distinguish a model with fast velocities and a long conduit from a model with slow velocities and a short conduit.

These results for the dispersion are also shown by the analytical expressions for the dispersion relations derived by Ferrazzini and Aki (1987). Fig. 12 plots the dispersion curves showing the ratio of the phase velocity to the acoustic velocity against the wavelength for the range of seismic parameters used in this study. For all acoustic velocities, the phase velocity decreases with wavelength. For the lowest acoustic velocity (Fig. 12), and highest volume of exsolved gas, the phase velocity of the slow wave decreases very slowly with increasing wavelength but remains close to the value of the acoustic velocity in the magma. In the numerical simulations, the low acoustic velocity showed no dispersion (Fig. 9a

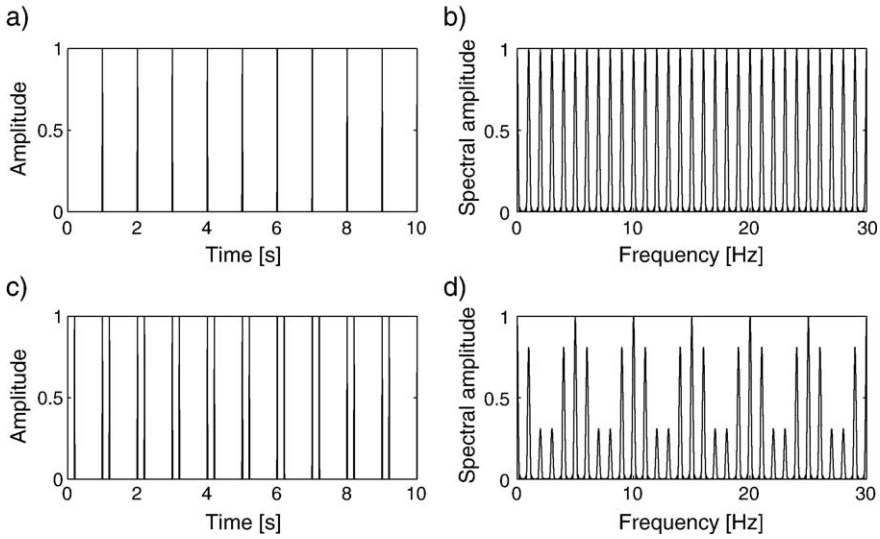

Fig. 11. The effect of the spacing of subevents on the amplitude of the spectral peaks. In (a), there are spikes spaced every 1 s and in spectrum (b), there are spectral peaks every 1 Hz all with the same amplitude. In (c), there are pairs of spikes spaced 0.2 s apart every 1 s, spectrum (d) shows spectral peaks every 1 Hz with amplitude highs every 5 Hz. If subevents arrive in pairs then a pattern of amplitude highs and lows is seen in the spectral peaks.

and b). As the acoustic velocity increases, the phase velocity decreases more rapidly with wavelength (Fig. 12) so that longer wavelengths travel slower relative to the acoustic velocity and this is seen as dispersion in the subevents in the numerical results (Fig. 9c, d and e).

Amplitude decay of the signal: When the seismic velocity is higher the signals decay more rapidly. For example, in Fig. 8b for an acoustic velocity of 400 ms^{-1} the amplitude of the subevents is very similar for the duration of the signal shown, while for Fig. 8e when the acoustic velocity is 2400 ms^{-1} the amplitude of the fourth subevent is about half of the amplitude of the second subevent. The seismic energy transmitted into the country rock when the seismic wave reaches the ends of the conduit depends on the contrast in the seismic parameters between the magma and the country

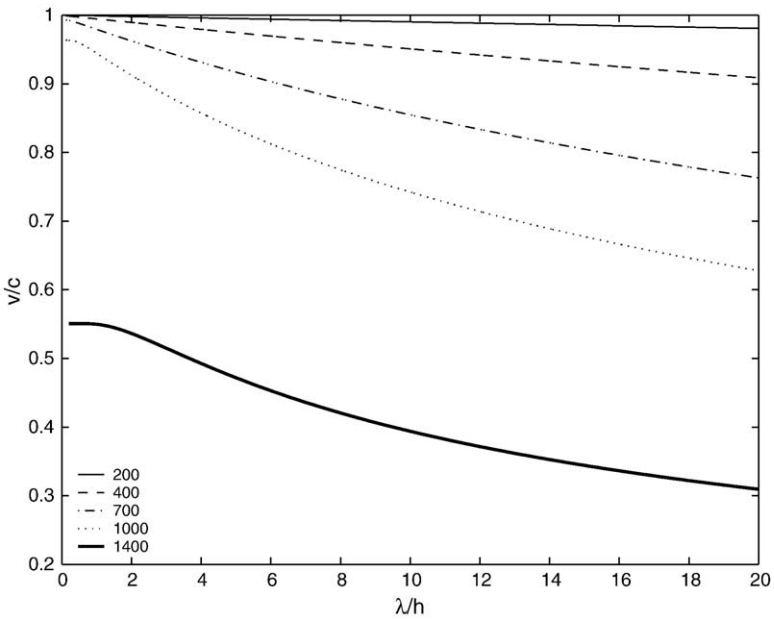

Fig. 12. Dispersion relations for a fluid-filled layer for seismic properties used in the numerical simulations. For a low acoustic velocity, there is very little dispersion and the phase velocity is similar to the acoustic velocity. As the acoustic velocity increases, there is strong inverse dispersion.

rock. For waves arriving at the boundary of the conduit at 90° to the interface, the fractions of energy reflected back into the conduit, E_R, and transmitted into the country rock, E_T, are given by

$$E_R = \left(\frac{\rho_s\alpha - \rho_f c}{\rho_s\alpha + \rho_f c}\right)^2, \quad (5)$$

and

$$E_T = \frac{4\rho_s\alpha\rho_f c}{(\rho_s\alpha + \rho_f c)^2}, \quad (6)$$

respectively, where c and ρ_f are the acoustic velocity and density of the magma, respectively, and α and ρ_s are the P-wave velocity and density of the country rock, respectively (Aki and Richards, 1980). If the acoustic velocity in the magma is similar to the P-wave velocity of the country rock, a higher fraction of the seismic energy escapes each time the seismic wave reaches the conduit ends and the signal decays more rapidly than for a lower acoustic velocity. For the acoustic velocity in the magma is different to the P-wave velocity of the country rock, a lower fraction of seismic energy escapes each time the wave is transmitted from the ends and the decay of the signal is slow because most of the wave remains trapped inside the conduit than for a higher acoustic velocity.

Subevents from the bottom of the conduit: When the acoustic velocity is low and the conduit is long a second set of subevents is present with a much lower amplitude (Fig. 6c, e and f). These subevents are transmitted into the country rock when the slow wave reaches the bottom of the conduit. They have a much lower amplitude because the bottom of the conduit is further from the 'seismometer' than the top of the conduit so the effect of geometrical spreading is greater. These smaller subevents are not seen for the higher acoustic velocity because the subevents from the top of the conduit are too closely merged.

7. Discussion

The results from the modelling show that the dispersion characteristics in the spectrograms depend on conduit length, seismic velocity and density contrast between the magma and the country rock. Using a series of schematic spectrograms based on numerical spectrograms (Fig. 13), it will now be demonstrated how a single low-frequency event can be constructed from a series of subevents leading to possible variations in its frequency history.

In the schematic spectrograms, the signals are allowed to decay more rapidly than the numerical results to take into account the effects of attenuation and three-dimensional geometrical spreading. These schematic spectrograms are then compared to spectrograms of observed low-frequency events from Montserrat to show how variations between different events can be explained in terms of variations in the acoustic velocity and conduit length.

7.1. Schematic spectrograms

The first spectrogram (Fig. 13a) shows low-frequency events from a short conduit with either a high or low acoustic velocity. Initially, the spectrogram contains high frequencies, the result of a broadband source signal. This part of the event decays rapidly and would result in a high-frequency start of a low-frequency event. There is also a lower frequency part, with a wavelength equal to the length of the conduit. This part forms the monochromatic coda of the event. If the conduit were made a bit longer (Fig. 13b), the event would show pulsing similar to Fig. 7a but the individual subevents are not separable.

Fig. 13c shows a series of subevents that leak from the top of the conduit. The conduit is longer than for Fig. 13a and b so the subevents are separable. The lack of dispersion indicates a system with a high impedance contrast so the acoustic velocity in the magma must be much lower than that of the country rock. Again, high frequencies are only seen at the start of the event because the high frequencies are attenuated more quickly than the low frequencies.

Fig. 13d shows an event composed of a series of repeated small dispersive subevents leaking from the top of the conduit. Again the conduit is longer than for Fig. 13a and b but similar to 13c. The dispersion is indicative of a low impedance contrast between the seismic properties of the magma and the country rock. The spacing of the subevents gives an idea of the ratio of the length of the conduit to the average velocity of the slow wave. High frequencies are seen only at the start of the event because high frequencies escape from the conduit more rapidly.

Fig. 13e shows the spectrogram for a similar long conduit with a high impedance contrast. There is no dispersion so all the frequencies arrive at the same time. Fig. 13f shows a single, very dispersive long event. This type of event might be formed if the conduit is very long and the impedance contrast is low. The wave has a long way to travel to the top of the conduit where energy can leak to the seismometers. This long distance

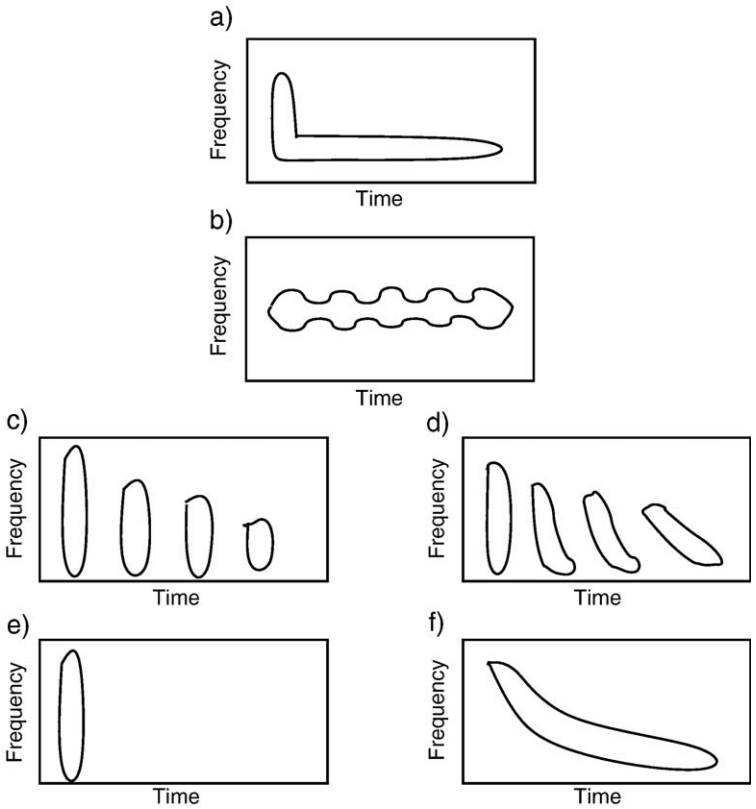

Fig. 13. Schematic spectrograms of possible ways of building a low-frequency event from subevents. (a) A short conduit section leads to a low-frequency oscillation combined with a higher frequency start, (b) a slightly longer conduit results in a pulsing effect but individual subevents cannot be separated, (c) a series of small events which are not dispersive from a longer conduit with a low acoustic velocity, (d) the low-frequency event is composed of a series of small dispersive events from a longer conduit with a high acoustic velocity, (e) a single event with no dispersion from a very long conduit with a low acoustic velocity, (f) the low-frequency event is a single long dispersive event from a very long conduit with a high acoustic velocity.

means that the faster high frequencies arrive before the slower low frequencies because they have the time to become widely separated, producing a long low-frequency event with a high frequency start. There is no second event because the conduit is so long that the seismic wave in the conduit has decayed before it arrives at the top of the conduit again. A long conduit would be required in this model. For this type of event, the spectrum of the signal would not be composed of equally spaced peaks.

7.2. Examples of observed low-frequency events

This section compares the spectra and spectrograms of recorded data from Soufrière Hills Volcano, Montserrat, with the numerical results in the previous sections. For each low-frequency event, the seismogram, spectrum and spectrogram are displayed. The spectra are plotted on a linear frequency scale so that equally spaced peaks can be readily identified. The logarithmic scale often used for plotting spectra makes it hard to identify peaks that are equally spaced.

The first two low-frequency events chosen for analysis are from a 20-min time period on 06/02/1997. These events were chosen because they showed different features to each other in the spectrograms. These events are similar to those described by Neuberg et al. (1998) and represent typical low-frequency events from Montserrat. The third event was chosen because it had spectral features similar to the numerical results. Similar events from the same swarm are described in Baptie et al. (2002) and are called ‘harmonic low-frequency events’ by the authors.

The low-frequency event in Fig. 14 has no high frequencies at the onset. Fig. 15 has an initially low-frequency onset and the high frequencies are delayed, arriving about 1 s after the beginning of the event. For the first event, the peak frequency is 1.2 Hz (Fig. 14b), and for the second event it is 1.5 Hz (Fig. 15b). Neither

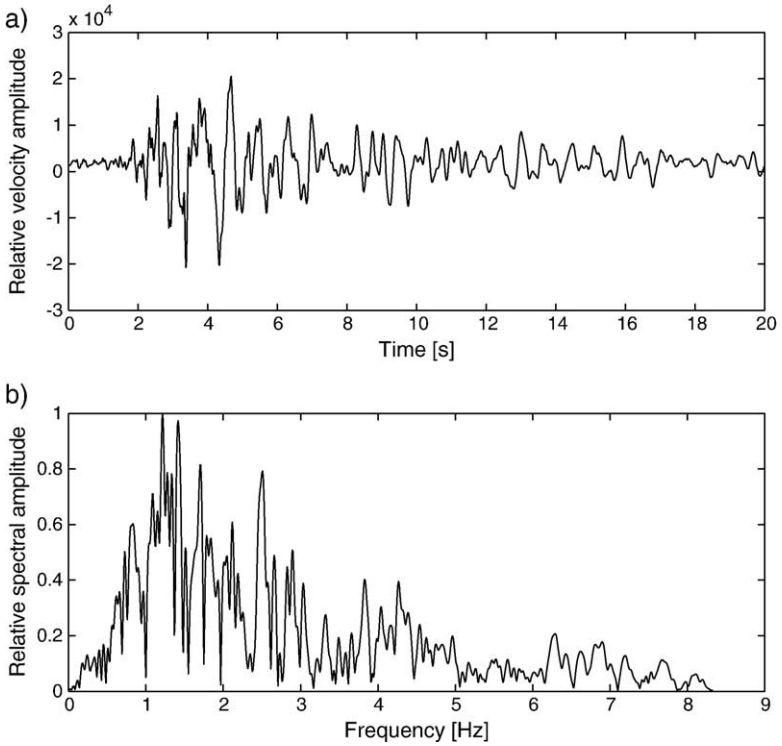

Fig. 14. Low-frequency event from Soufrière Hills Volcano, Montserrat. This event shows no high-frequency onset and while the spectrum shows sharply defined peaks, these are not equally spaced. Low-frequency event from station MBGA, recorded on 06/02/1997.

of the spectra have a series of equally spaced peaks, unlike the spectra from the numerical modelling but have sharply defined peaks with no clear repetitive pattern. The final low-frequency event (Fig. 16) is considerably longer than the other events. Its spectrum shows a series of equally spaced peaks approximately 1

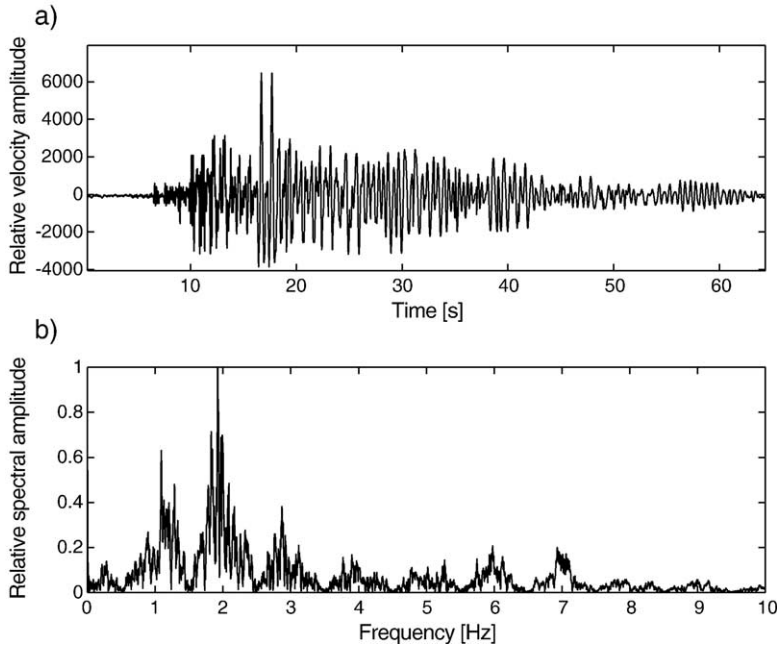

Fig. 15. Low-frequency event showing high frequencies lasting just under 1 s arriving after the start of the event. Low-frequency event from station MBGA, Montserrat, recorded on 06/02/1997.

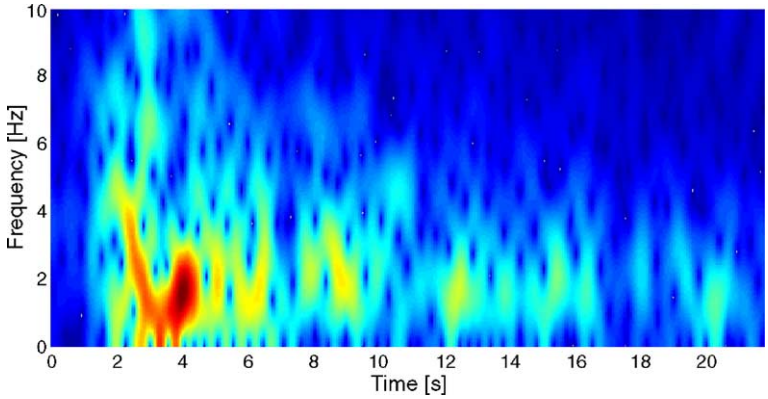

Fig. 16. Harmonic low-frequency event with a long duration. The spectra show closely spaced peaks which are not equally spaced superimposed on harmonic spectral peaks spaced approximately every 1 Hz. From station MBWH, Montserrat, recorded on 13/08/1997.

Hz apart superimposed on irregularly spaced peaks which are much closer together.

Fig. 17 shows the spectrogram for the low-frequency event in Fig. 14. This low-frequency event consists of one main high amplitude subevent lasting just over 2 s. The high frequencies of this subevent arrive before the low frequencies. After this, there are a few smaller subevents. The single subevent shows dispersion in a pattern similar to Fig. 13f. There is a time delay of 2 s between the arrival of the 4 Hz part of the event and the 1 Hz part of the event. The dispersion suggests that the impedance contrast between the seismic properties of the magma and those of the country rock must be low.

Fig. 18 is the spectrogram for the low-frequency event in Fig. 15a. The event consists of an initial subevent, for which the low frequencies arrive slightly earlier than the high frequencies, followed by a second subevent, for which the high frequencies arrive slightly before low frequencies. This subevent occurs 2 s after the first subevent. After this, there are several smaller subevents. The dispersion in the low-frequency event is not as simple as the dispersion in the numerical models but it does appear to show dispersion consistent with that of slow waves. The first subevent has a low-frequency onset. In the second subevent, the high frequencies arrive first, so the high frequencies must travel quicker than the low frequencies, as a result of inverse dispersion. The dispersion in the event is similar to the schematic diagram in Fig. 13d.

The spectrogram of the harmonic low-frequency event (Fig. 19) is made using a longer time window because it does not separate into subevents and the longer window length gives better frequency resolution. The spectrogram shows bands approximately 1 Hz apart that pulse with time. The spectrogram is similar to the schematic diagram (Fig. 13b).

The short-windowed spectrograms highlight the variability of the individual low-frequency events. All the events have a more complex structure than the synthetic seismograms. The low-frequency events are generally made up of a series of subevents suggesting that they are the result of the slow wave leaking from the ends of

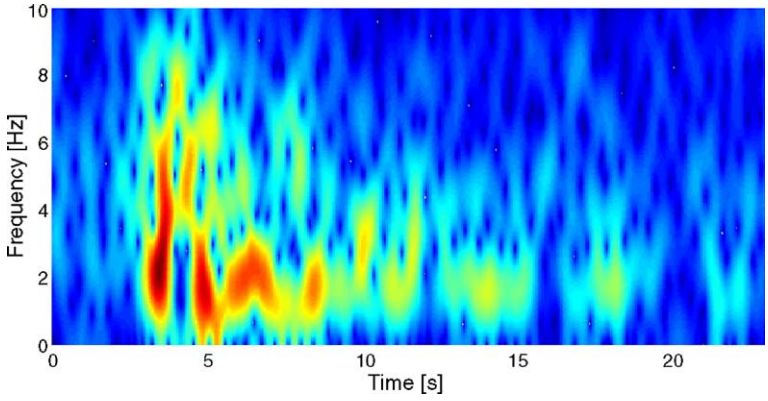

Fig. 17. Spectrogram of the low-frequency event in Fig. 14. This event consists of one main subevent showing inverse dispersion. The window length of the spectrogram is 1 s.

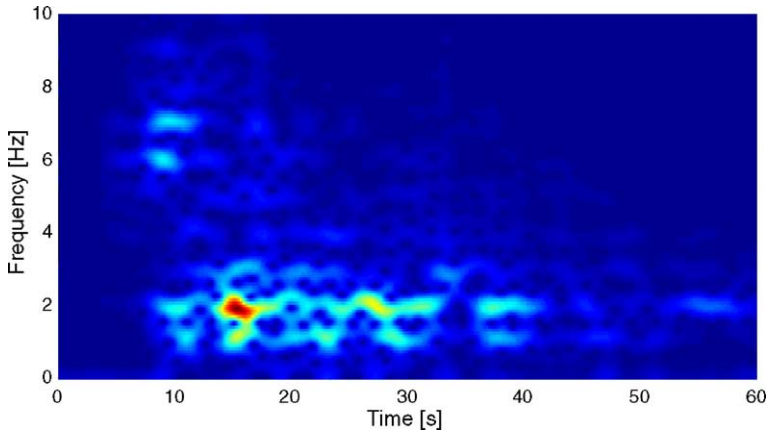

Fig. 18. Spectrogram of the low-frequency event in Fig. 15. This event consists of two subevents showing slight inverse dispersion. The window length of the spectrogram is 1 s.

the conduit. The harmonic low-frequency event (Fig. 19) has subevents that are so closely merged they cannot be separated, producing a 'tornillo'-like event. In the observational data, the high frequencies decay more rapidly than the lower frequencies due to attenuation so the dispersion in the subevents is harder to identify. Many low-frequency events at other volcanoes, such as those at Redoubt volcano (Chouet, 1996) and Galeras (Gil Cruz and Chouet, 1997) are similar to those on Montserrat in that they do not have sharply defined, regularly spaced spectral peaks. However, one class of low-frequency events does show similar spectra to those of the numerical models. Tornillos, described by Gòmez and Torres (1997) show sharply defined spectral peaks and a spectrogram of a monochromatic tornillo would be similar to Fig. 13d.

There are two ways of creating differences in the timing of the arrival of subevents. Figs. 14 and 15 show subsequent seismic event 20 min apart. If the low-frequency events came from the same part of the conduit, the variation in the spectrograms would be caused by temporal variations in the seismic properties of the magma. The low-frequency event in Fig. 14 shows more dispersion and the subevents are more widely spaced than the low-frequency event in Fig. 15. To have more dispersion, the acoustic velocity must be higher for the first than the second. If this were the case then the event spacing would decrease rather than increase. This means the observations are inconsistent with the seismic properties varying with time.

Alternatively, the conduit is split into several sections and the low-frequency events were triggered in

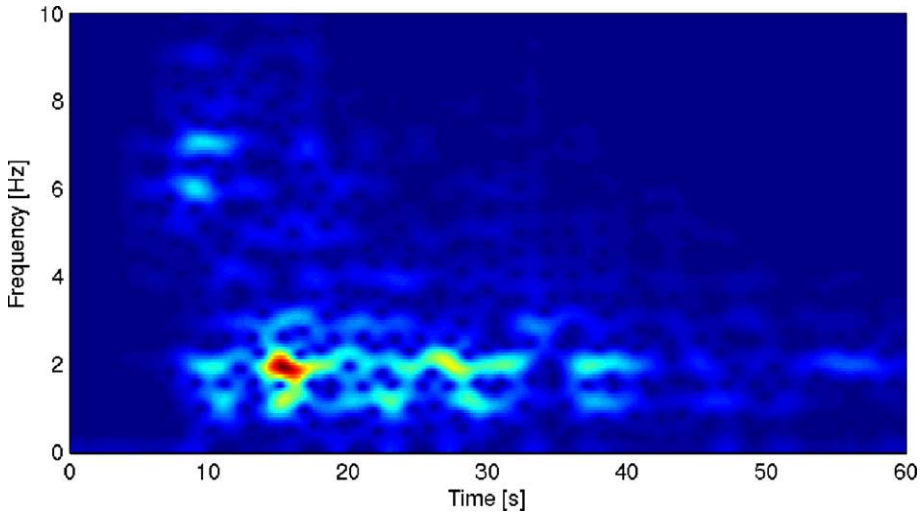

Fig. 19. Spectrogram of the harmonic low-frequency event in Fig. 16. The spectrogram does not show clearly defined subevents but rather continuous peaks about 1 Hz apart. The window length for this spectrogram is 2 s.

different parts of the conduit. Each conduit section resonates independently of the others, and has different dimensions and seismic properties to the other sections thus producing variations in the time–frequency behaviour of the low-frequency events. The low-frequency event in Fig. 14 therefore occurred in a longer conduit section with a higher acoustic velocity than the conduit section resulting in the low-frequency event in Fig. 15.

The slow attenuation of the last event (Fig. 16) suggests that the acoustic velocity is much lower than for the other low-frequency events. Subevents cannot be separated indicating that a short conduit section is resonating. This low-frequency event occurred several months after the others shown in this study. The difference could be due to either a different part of the conduit resonating or a temporal variation in the seismic properties of the magma. Analysis of more low-frequency events between the two dates is needed to distinguish between these possibilities.

Reasons for the additional complexity of real events: If low-frequency events are composed of small equally spaced subevents, then the spectrum of the seismogram of a single event should also show a series of equally spaced spikes. The timing of the subevents in the observed low-frequency events is not regular explaining the lack of regular peaks in the spectra of the whole events. Even the low-frequency event in Fig. 14, which is similar to Fig. 13f, has further lower amplitude subevents. Some of the complexities that could cause these differences are:

1. Variations in the geometry of conduit could create different dispersion patterns and patterns of leakage from the conduit. The finite difference code is two-dimensional. This limits the number of sets of repetitive frequency peaks superimposed. In reality, the system is three-dimensional and there could be multiple sets of repetitive frequency peaks superimposed instead of two. Having multiple sets of super-imposed peaks may make it harder to identify each individual set.
2. Inhomogeneities in the country rock may create a series of small events which are closely merged and irregularly spaced. The reason for the equal spacing of the peaks in frequency in the synthetic models, is that the subevents arrive exactly spaced in time, because they always leak from the top of the conduit and have travelled the same distance in between. If these subevents were to arrive at random time intervals, the spectrum would be like a brush with irregularly spaced sharply defined peaks (Neuberg and Luckett, 1996). The spectra in Figs. 14 and 15 can both be described as brush-like. An irregular spacing of the subevents with time could be produced if rather than escaping from the ends of the conduit, there are seismic layers on the outside of the conduit. The signal would be built up of small subevents from each boundary between seismic layers. Provided these are not equally spaced, the subevent spacing will be irregular.

8. Conclusions

The numerical results show that the dispersion is dependent on the contrast in seismic parameters between the conduit and the country rock. The spectra of the events are simple, showing a series of regularly spaced peaks. As the impedance contrast decreases, the slow wave travels slower relative to the acoustic velocity and the subevents are more dispersive with the low frequencies travelling slower than high frequencies. The spacing of subevents depends on the conduit length. As the conduit length is made shorter, the subevents merge eventually producing a ‘tornillo’-like event.

Low-frequency events from Soufrière Hills Volcano do not have simple spectra consisting of a series of equally spaced peaks. Therefore, they are not made up of regularly spaced smaller events. Short-windowed spectrograms show that each low-frequency event is composed of a series of subevents that are irregularly spaced.

From the short-windowed spectrograms, it is possible to estimate the spacing of events with time and in some cases identify dispersion within the system. The transforms allow the identification of differences between low-frequency events in terms of dispersion and the number and timing of the events. These differences suggest that low-frequency events form in different parts of the conduit and that there are temporal variation in the events.

Acknowledgements

This work was funded by the U.K. National and Environmental Research Council through PhD grant GT 04/99/ES/117.

References

Aki, K., Richards, P., 1980. Quantitative Seismology: Theory and Methods. W.H. Freeman and Company, New York.

Baptie, B., Luckett, R., Neuberg, J., 2002. Observations of low-frequency earthquakes and volcanic tremor at Soufrière Hills Volcano, Montserrat. In: Druitt, T.H., Kokelaar, B.P. (Eds.), The Eruption of the Soufrière Hills Volcano, Montserrat, from 1995 to 1999. Memoirs, Geological Society, London, pp. 611–620.

Benoit, J., McNutt, S., 1997. New constraints on source processes of volcanic tremor at Arenal Volcano, Costa Rica, using broadband seismic data. Geophys. Res. Lett. 24, 449–452.

Cerjan, C., Kosloff, D., Kosloff, R., Reshef, M., 1985. A nonreflecting boundary condition for discrete acoustic and elastic wave equations. Geophysics 50, 705–708.

Chouet, B.A., 1986. Dynamics of a fluid-driven crack in three dimensions by the finite difference method. J. Geophys. Res. 91, 13967–13992.

Chouet, B.A., 1988. Resonance of a fluid-driven crack: radiation properties and implications for the source of long-period events and harmonic tremor. J. Geophys. Res. 93, 4375–4400.

Chouet, B., 1996. Long period seismicity: its source and use in eruption forecasting. Nature 380, 309–316.

Devine, J.D., Murphy, M.D., Rutherford, M.J., Barclay, J., Sparks, R.S.J., Carroll, M.R., Young, S.R., Gardner, J.C., 1998. Petrological evidence for pre-eruptive pressure–temperature conditions and recent reheating, of andesitic magma erupting at Soufriere Hills Volcano, Montserrat, WI. J. Geophys. Res. 25, 3669–3672.

Ferrazzini, V., Aki, K., 1987. Slow waves trapped in a fluid-filled crack: implications for volcanic tremor. J. Geophys. Res. 92, 9215–9223.

Gil Cruz, F., Chouet, B.A., 1997. Long-period events, the most characteristic seismicity accompanying the emplacement and extrusion of a lava dome in Galeras Volcano, Columbia in 1991. J. Volcanol. Geotherm. Res. 77, 121–158.

Gòmez, D.M., Torres, R.A., 1997. Unusual low-frequency events with slowly decaying coda waves observed at Galeras and other volcanoes. J. Volcanol. Geotherm. Res. 77, 173–193.

Hagerty, M.T., Schwartz, S.Y., Garces, M.A., Protti, M., 2000. Analysis of seismic and acoustic observations and Arenal Volcano, Costa Rica, 1995–1997. J. Volcanol. Geotherm. Res. 101, 27–65.

Johnson, J.B., Lees, J.M., 2000. Plugs and chugs—seismic and acoustic observations of degassing at Karymsky, Russia and Sangay, Ecuador. J. Volcanol. Geotherm. Res. 101, 67–82.

Jousset, P., Neuberg, J., Sturton, S., 2003. Modelling the time-dependent frequency content of low-frequency volcanic earthquakes. J. Volcanol. Geotherm. Res. 128, 201–223.

Levander, A.R., 1988. Fourth-order finite-difference P–SV seismograms. Geophysics 53, 1425–1436.

Miller, A.D., Stewart, R.C., White, R.A., Luckett, R., Baptie, B.J., Aspinall, W.P., Latchman, J.L., Lynch, L.L., Voight, B., 1998. Seismicity associated with dome growth and collapse at the Soufrière Hills Volcano, Montserrat. Geophys. Res. Lett. 25, 3401–3404.

Neuberg, J., 2000. Characteristics and causes of shallow seismicity in andesitic volcanoes. Philos. Trans. R. Soc. Lond., A 358, 1533–1546.

Neuberg, J., Luckett, R., 1996. Seismo-volcanic sources on Stromboli volcano. Annal. Geofis. 39, 377–391.

Neuberg, J., O'Gorman, C., 2002. A model of the seismic wavefield in gas-charged magma: application to the Soufrière Hills Volcano, Montserrat. In: Druitt, T.H., Kokelaar, B.P. (Eds.), The Eruption of the Soufriere Hills Volcano, Montserrat, from 1995 to 1999. Memoirs, Geological Society, London, pp. 603–609.

Neuberg, J., Baptie, B., Luckett, R., Stewart, R., 1998. Results from the broadband seismic network on Montserrat. Geophys. Res. Lett. 25, 3661–3664.

Neuberg, J., Luckett, R., Baptie, B., Olsen, K., 2000. Models of tremor and low-frequency earthquake swarms on Montserrat. J. Volcanol. Geotherm. Res. 101, 83–104.

Powell, T., Neuberg, J., 2003. Time dependent features in tremor spectra. J. Volcanol. Geotherm. Res. 128, 177–185.

Rivers, M.L., Carmichael, I.S.E., 1987. Ultrasonic studies of silicate melts. J. Geophys. Res. 92, 9247–9270.

Rowe, C.A., Aster, R.C., Kyle, P.R., Dibble, R.R., Schlue, J.W., 2000. Seismic and acoustic observations at Mount Erebus Volcano, Ross Island, Antarctica, 1994–1998. J. Volcanol. Geotherm. Res. 101, 105–128.

Schlindwein, V., Wassermann, J., Scherbaum, F., 1995. Spectral analysis of harmonic tremor signals at Mt. Semeru volcano, Indonesia. Geophys. Res. Lett. 22, 1685–1688.

Sturton, S., 2003. Modelling volcanic earthquakes and tremor. Unpublished PhD Thesis, University of Leeds.

Watts, R.B., Herd, R.A., Sparks, R.S.J., Young, S.R., 2002. Growth patterns and emplacement of the andesitic lava dome at Soufrière Hills Volcano, Montserrat. In: Druitt, T.H., Kokelaar, B.P. (Eds.), The Eruption of the Soufrière Hills Volcano, Montserrat, from 1995 to 1999. Memoirs, Geological Society, London, pp. 115–152.